Massively Scalable Inverse Reinforcement Learning in Google Maps

Matt Barnes[1]* **Matthew Abueg**[1]*

Oliver F. Lange[2] **Matt Deeds**[2] **Jason Trader**[2]

Denali Molitor[1] **Markus Wulfmeier**[3]† **Shawn O'Banion**[1]†

[1]Google Research [2]Google Maps [3]Google DeepMind

Abstract

Inverse reinforcement learning (IRL) offers a powerful and general framework for learning humans' latent preferences in route recommendation, yet no approach has successfully addressed planetary-scale problems with hundreds of millions of states and demonstration trajectories. In this paper, we introduce scaling techniques based on graph compression, spatial parallelization, and improved initialization conditions inspired by a connection to eigenvector algorithms. We revisit classic IRL methods in the routing context, and make the key observation that there exists a trade-off between the use of cheap, deterministic planners and expensive yet robust stochastic policies. This insight is leveraged in Receding Horizon Inverse Planning (RHIP), a new generalization of classic IRL algorithms that provides fine-grained control over performance trade-offs via its planning horizon. Our contributions culminate in a policy that achieves a 16-24% improvement in route quality at a global scale, and to the best of our knowledge, represents the largest published benchmark of IRL algorithms in a real-world setting to date. We conclude by conducting an ablation study of key components, presenting negative results from alternative eigenvalue solvers, and identifying opportunities to further improve scalability via IRL-specific batching strategies.

1 Introduction

Inverse reinforcement learning (IRL) is the problem of learning latent preferences from observed sequential decision making behavior. First proposed by Rudolf Kálmán in 1964 (when it went under the name of inverse optimal control [23], and later structural estimation [39]), IRL has now been studied in robotics [1, 35, 33], cognitive science [3], video games [43, 45], human motion behavior [26, 36] and healthcare [22, 52], among others.

In this paper, we address a key challenge in all these applications: scalability [7, 30, 49]. With several notable exceptions, IRL algorithms require solving an RL problem at every gradient step, in addition to performing standard backpropagation [15, 41]. This is a significant computational challenge, and necessitates access to both an interactive MDP and a dataset of expert demonstrations that are often costly to collect. By addressing the scalability issue, we aim to leverage recent advancements in training foundation-sized models on large datasets.

To illustrate our claims, we focus on the classic route finding task, due to its immediate practical significance and the availability of large demonstration datasets. Given an origin and destination location anywhere in the world, the goal is to provide routes that best reflect travelers' latent preferences.

* †Equal contribution. Correspondence to {mattbarnes,mattea,mwulfmeier,obanion}@google.com

NeurIPS 2023 Workshop on Generalization in Planning (GenPlan 2023).

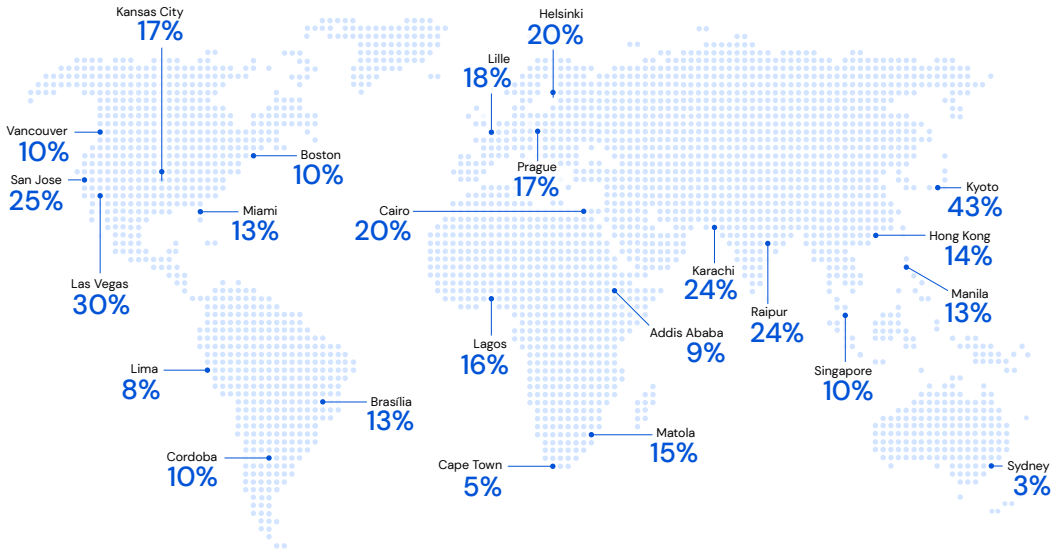

Figure 1: Google Maps route accuracy improvements in several world regions, when using our inverse reinforcement learning policy. Full results are presented in Table 1 and Figure 7.

These preferences are only observed through their physical behavior, which implicitly trade-off factors including traffic conditions, distance, hills, safety, scenery, road conditions, etc. Although we primarily focus on route finding, the advancements in this paper are general enough to find use more broadly.

We address the scalability challenge by providing both (a) practical techniques to improve IRL scalability and (b) a new view on classic IRL algorithms that reveals a novel generalization and enables fine-grained control of performance characteristics. Concretely, our contributions are as follows:

- **MaxEnt++** An improved version of MaxEnt IRL [54] that is inspired by a connection to dominant eigenvectors to initialize the backward pass closer to the desired solution.
- **Spatial parallelization** A simple, practical technique to shard the global MDP by leveraging a geography-based sparse mixture-of-experts.
- **Graph compression strategies** Lossless and lossy methods to compress the graph matrices and reduce both the memory footprint and FLOP count across all IRL algorithms.
- **Receding Horizon Inverse Planning (RHIP)** A novel IRL algorithm that generalizes MaxEnt++, BIRL [32] and MMP [34]. RHIP leverages our insight that there exists a trade-off between the use of cheap, deterministic planners and expensive yet robust stochastic policies, and enables fine-grained control over accuracy and planning time characteristics.
- **Alternative solvers** Secondary negative results when attempting to use Arnoldi iteration and a closed-form matrix geometric series in MaxEnt, which we defer to Appendix A.
- **MaxEnt theory** Secondary theoretical analyses of MaxEnt, which we defer to Appendix B.

Our work culminates in a global policy that achieves a 15.9% and 24.1% lift in route accuracy for driving and two-wheelers, respectively (Figure 1), and was successfully applied to a large scale setting in Google Maps. To the best of our knowledge, this represents the largest published benchmark of IRL algorithms in a real-world setting to date.

2 Related Work

IRL approaches can be categorized according to the form of their loss function.[2] MaxEnt [54] optimizes cross-entropy loss, MMP [34] optimizes margin loss, and BIRL [32] optimizes sequential Bayesian likelihood. LEARCH [35] replaces the quadratic programming optimization in MMP [34]

[2]The IRL route optimization problem is reducible to supervised classification with infinitely many classes, where each class is a valid route from the origin to the destination, the features are specified by the edges, and the label is the demonstration route. Unlike typical supervised learning problems, solving this directly by enumerating all classes is intractable, so IRL approaches take advantage of the MDP structure to efficiently compute loss gradients.

with stochastic gradient descent. Choi and Kim [9] replace the MCMC sampling in BIRL [32] with maximum a posteriori estimation. Extensions to continuous state-action spaces are possible through sampling-based techniques [14]. Our work builds on Wulfmeier, Ondruska, and Posner [47] and Mainprice et al. [29], who applied MaxEnt and LEARCH to the deep function approximator setting.

Existing approaches to scale IRL consider several orthogonal and often complimentary techniques. Michini, Cutler, and How [30] incorporate real-time dynamic programming [4], which is less applicable with modern accelerators' matrix operation parallelization. Chan and Schaar [7] apply a variational perspective to BIRL, which reduces computational cost but adds considerable algorithmic complexity and requires tuning in comparison to the maximum a posteriori version. MMP is inherently more scalable, as its inner loop only requires calling a planning subroutine (e.g. Dijkstra) [35]. However, it lacks robustness to real-world noise, and has lost favor to more stable and accurate probabilistic policies [31]. MacGlashan and Littman [28] similarly introduce a receding horizon to improve planning times.[3] They assume zero reward beyond the horizon, whereas we assume a cheap deterministic planner beyond the horizon and a more expensive stochastic planner elsewhere. This is necessary to propagate rewards from distant goal states.

Recently, imitation learning approaches that directly attempt to recover the demonstrator policy have gained increased attention [18, 24]. Behavior cloning avoids performing potentially expensive environment roll-outs, but suffers regret quadratic in the horizon [37]. DAGGER solves the compounding errors problem by utilizing expert corrections [38]. IRL also addresses the compounding errors issue but without repeated expert involvement, although can be expensive as it requires solving the RL problem as a subroutine. Recent approaches use the demonstrators' distribution to reduce exploration in the RL subroutine [41] and are complementary to our work. Mixed approaches such as GAIL simultaneously learn both a policy (generator) and reward function (discriminator) [15, 18, 24]. We avoid explicitly learning a policy to bypass instabilities of adversarial training [51] and due to the *goal conditioning* requirement discussed in Section 3.

3 Inverse Reinforcement Learning

A Markov decision process (MDP) $\mathcal{M}$ is defined by a discrete set of states $\mathcal{S}$, actions $\mathcal{A}$, transition kernel $\mathcal{T}$ and reward function r (i.e. negative cost function). Given $\mathcal{M} \setminus r$ and a set of state-action trajectory demonstrations $\mathcal{D} = \{\tau_1, ..., \tau_N\}$ sampled from a demonstration policy π_E, the goal of IRL is to recover the latent r.[4] We denote the state and state-action distributions of trajectory τ by ρ_τ^s and ρ_τ^{sa}, respectively.

For expository purposes, we initially restrict our attention to the classic path-planning problem, and discuss extensions in Section 6. In line with prior work [54], we define these MDPs as discrete, deterministic, and undiscounted where $r_\theta(s_i, s_j) \leq 0$ denotes the θ-parameterized reward of transitioning from state s_i to state s_j and non-allowable transitions have reward $-\infty$. There exists a single self-absorbing zero-reward destination state s_d, which implies that each unique destination induces a slightly different MDP. However, for the sake of notational simplicity and without loss of generality, we consider the special case of a single origin state s_o and single destination state s_d. We do not make this simplification for any of our empirical results. In the path-planning context, states (i.e. nodes) represent road segments and allowable transitions (i.e. edges) between nodes represent turns.

Inverse reinforcement learning algorithms follow the two-player zero-sum game

$$\min_{\pi \in \Pi} \max_{\theta \in \Theta} J(\pi_E, r_\theta) - J(\pi, r_\theta) = \min_{\pi \in \Pi} \max_{\theta \in \Theta} f(\pi_E, \pi, r_\theta) \tag{1}$$

where $J(\pi, r_\theta) = \mathbb{E}_{\tau \sim \pi} \sum_{(s_t, s_{t+1}) \in \tau} r_\theta(s_t, s_{t+1})$ denotes the value of the policy π under reward function r_θ. We consider primal strategies for the equilibrium computation, where the policy player follows a no-regret strategy against a best-response discriminative player [42]. Classic IRL algorithms follow from Equation 1 by specifying certain policy classes and regularizers (see Appendix C for details). Following Ziebart et al. [54], we refer to the *backward pass* as estimating the current policy π and the *forward pass* as rolling out the current policy. The backward pass runtime in MMP and BIRL is governed by Dijkstra's algorithm, whereas the convergence of MaxEnt's backward pass is governed by the graph's second largest magnitude eigenvalue (see Theorem B.3).

Goal conditioning Learning a function r_θ using IRL provides a concise representation of preferences and simplifies transfer across goal states s_d, as the reward function is decomposed into

[3] MacGlashan and Littman [28] reduces to BIRL [32] with infinite horizon.

[4] This is an ill-conditioned problem, as multiple reward functions can induce the same trajectories. Methods impose regularization or constraints to form a unique solution, e.g. the principle of maximum entropy [54].

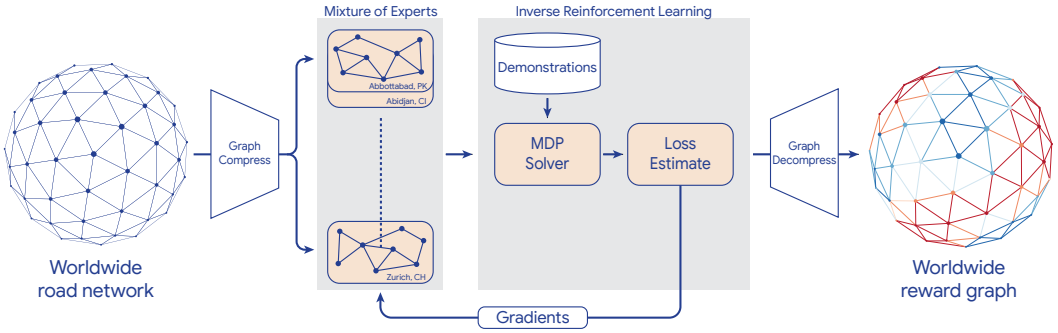

Figure 2: Architecture overview. The final rewards are used to serve online routing requests.

a general learned term and a fixed modification at the destination (self-absorbing, zero-reward). In the tabular setting, the number of reward parameters is $\mathcal{O}(SA)$ even when conditioning on s_d. This is in contrast to approaches that explicitly learn a policy or Q-function (e.g. BC, IQ-Learn [16], GAIL [18], DAGGER [37]), which require additional complexity when conditioning on s_d, e.g. in the tabular setting, the number of policy parameters increases from $\mathcal{O}(\mathcal{SA})$ to $\mathcal{O}(S^2A)$. By learning rewards instead of policies, we can evaluate r_θ *once offline* for every edge in the graph, store the results in a database, precompute contraction hierarchies [17], and use a fast graph search algorithm to find the highest reward path[5] for online (s_o,s_d) requests. This is in contrast to a learned policy, which must be evaluated *online for every* (s_o,s_d) *request* and for every step in the sampled route – a computationally untenable solution in many online environments.

4 Methods

The worldwide road network contains hundreds of millions of nodes and edges. At first glance, even attempting to fit the graph features into high-bandwidth memory to compute a single gradient step is infeasible. In this section, we present a series of advancements which enable solving the world-scale IRL route finding problem, summarized in Figure 2. At the end of Section 6, we provide a useful summary of other directions which yield negative results.

Parallelism strategies We use a sparse Mixture of Experts (MoE) strategy [40], where experts are uniquely associated to geographic regions and each demonstration sample is deterministically assigned to a single expert (i.e. one-hot sparsity). This minimizes cross-expert samples and allows each expert to learn routing preferences specific to its region. Specifically, we shard the global MDP $\mathcal{M}$ and demonstration dataset $\mathcal{D}$ into m disjoint subproblems $(\mathcal{M}_1,\mathcal{D}_1),\ldots,(\mathcal{M}_m,\mathcal{D}_m)$. We train region-specific experts $r_{\theta_1},\ldots,r_{\theta_m}$ in parallel, and compute the final global rewards using $r(s,a)=r_{\theta_i}(s,a)$ where $(s,a)\in\mathcal{M}_i$. We additionally use standard data parallelism strategies within each expert to further partition minibatch samples across accelerator devices.

MaxEnt++ initialization MaxEnt [54] is typically initialized to the value (i.e. log partition) function $v^{(0)}(s_i)=\log\mathbb{I}[s_i=s_d]$, where $\mathbb{I}[s_i=s_d]$ is zero everywhere except at the destination node (see Appendix C.1). This propagates information outwards from the destination, and requires that the number of dynamic programming steps is at least the graph diameter for arbitrary destinations. Instead, we initialize the values $v^{(0)}$ to be the *highest reward to the destination from every node*. This initialization is strictly closer to the desired solution v by

$$\underbrace{\mathbb{I}[s_i=s_d]}_{\text{MaxEnt initialization}} \leq \underbrace{\min_{\tau\in\mathcal{T}_{s_i,s_d}} e^{r(\tau)}}_{\text{MaxEnt++ initialization}} \leq \underbrace{\sum_{\tau\in\mathcal{T}_{s_i,s_d}} e^{r(\tau)}=v(s_i)}_{\text{Solution}} \tag{2}$$

where $\mathcal{T}_{s_i,s_d}$ is the (infinite) set of all paths which begin at s_i and end at s_d (see proof in Appendix B.3). Note that equality only holds on contrived MDPs, and the middle term can be cheaply computed via Dijkstra or A*. We call this method MaxEnt++ (summarized in Algorithm 2).[6]

[5] The highest reward path is equivalent to the *most likely* path under MaxEnt [54].

[6] a nod to the improved initialization of k-means++ [2].

Algorithm 1 RHIP (Receding Horizon Inverse Planning)

Input: Current reward r_θ, horizon H,
demonstration τ with origin s_o and destination s_d
Output: Parameter update $\nabla_\theta f$

`# Policy estimation`
$v^{(0)}(s) \leftarrow \text{DIJKSTRA}(r_\theta, s, s_d)$
$\pi_d(a|s) \leftarrow \text{Greedy}(r_\theta(s,a) + v^{(0)}(s'))$
for $h = 1,2,...,H$ **do**
  $Q^{(h)}(s,a) \leftarrow r_\theta(s,a) + v^{(h-1)}(s')$
  $v^{(h)}(s) \leftarrow \log \sum_a \exp Q^{(h)}(s,a)$
end for
$\pi_s(a|s) \leftarrow \frac{\exp Q^{(H)}(s,a)}{\sum_{a'} \exp Q^{(H)}(s,a')}$
$\pi \leftarrow \left[(\pi_s)_{\times H}, (\pi_d)_{\times \infty}\right]$ ▷ Equation 3

`# Roll-out` $\pi_s \to \pi_d$
$\rho^{sa}_\theta \leftarrow \text{Rollout}(\pi, \rho^s_\tau)$
$\rho^{sa}_* \leftarrow \text{Rollout}(\pi_{2:\infty}, \rho^s_{\tau_{2:\infty}}) + \rho^{sa}_\tau$

$\nabla_\theta f \leftarrow \sum_{s,a} (\rho^{sa}_*(s,a) - \rho^{sa}_\theta(s,a)) \nabla_\theta r_\theta(s,a)$
Return: $\nabla_\theta f$

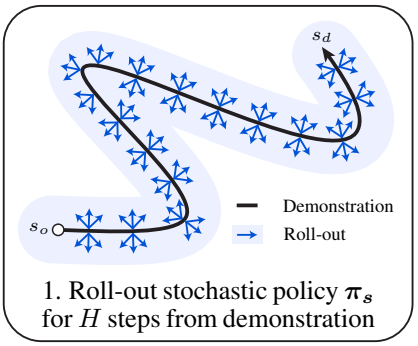

1. Roll-out stochastic policy $\boldsymbol{\pi_s}$ for H steps from demonstration

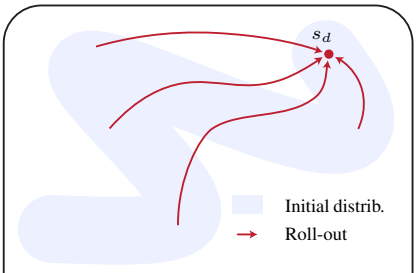

2. Continue roll-out with deterministic policy $\boldsymbol{\pi_d}$

Figure 3: RHIP rolls out the computationally expensive stochastic policy π_s for H steps from the demonstration path before transitioning to the cheaper deterministic policy π_d, as described in Equation 3. DIJKSTRA computes the highest reward path from state s to s_d under r_θ. $\text{Greedy}(Q(s,a)) \in \{0,1\}$ is the deterministic policy that selects the action with the highest Q-value. $\text{Rollout}(\pi, \rho^s) = \rho^{sa}$ computes the state-action distribution ρ^{sa} from rolling out the policy π from the initial state distribution ρ^s until convergence to the destination s_d.

The correspondence between MaxEnt and power iteration provides a more intuitive perspective. Specifically, the MaxEnt backward pass initialization $e^{v^{(0)}}$ defines the initial conditions of power iteration, and the solution e^v is the dominant eigenvector of the graph. By more closely aligning the initialization $v^{(0)}$ to the solution, the number of required power iteration steps is decreased.

Receding Horizon Inverse Planning (RHIP) In this section, our key insight is that classic IRL algorithms exhibit a trade-off between the use of cheap, deterministic planners (e.g. MMP [34]) and the use of expensive yet robust stochastic policies (e.g. MaxEnt [54]). This insight reveals a novel generalized algorithm that enables fine-grained control over performance characteristics and provides a new view on classic methods.

First, let π_s denote the stochastic policy after H steps of MaxEnt++ and π_d denote the deterministic policy that follows highest reward path, i.e. $\pi_d(a|s) \in \{0,1\}$. Let $\mathcal{T}_{s,a}$ denote the set of all paths which begin with state-action pair (s,a). We introduce a new policy defined by

$$\pi(a|s) \propto \sum_{\tau \in \mathcal{T}_{s,a}} \underbrace{\pi_d(\tau_{H+1})}_{\text{Deterministic policy}} \prod_{h=1}^{H} \underbrace{\pi_s(a_h|s_h)}_{\text{Stochastic policy}} . \tag{3}$$

The careful reader will notice that Equation 3 reduces to classic IRL algorithms for various choices of H. For $H=\infty$ it reduces to MaxEnt++, for $H=1$ it reduces to BIRL [32], and for $H=0$ it reduces to MMP [34] with margin terms absorbed into r_θ (see Appendix C for details).

We call this generalization Receding Horizon Inverse Planning (RHIP, pronounced *rip*). As described in Algorithm 1, RHIP performs H backup steps of MaxEnt++, rolls out the resulting stochastic policy π_s for H steps, and switches to rolling out the deterministic policy π_d until reaching the destination. The receding horizon H controls RHIP's compute budget by trading off the number of stochastic and deterministic

Table 1: Route quality of manually designed and IRL baselines. Due to the high computational cost of training the global model (bottom 3 rows), we also evaluate in a smaller, more computationally tractable set of metros (top section). Metrics are NLL (negative log-likelihood), Acc (accuracy, i.e. perfect route match) and IoU (Intersection over Union of trajectory edges). Numbers in bold are statistically significant with p-value less than .122 (see Appendix D.3). Two-wheeler data is unavailable globally.

		Drive			Two wheelers		
Policy class	Reward r_θ	NLL	Acc	IoU	NLL	Acc	IoU
ETA	Linear		.4034	.6566		.4506	.7050
ETA+penalties	Linear		.4274	.6823		.4475	.7146
MMP/LEARCH [34, 35]	Linear		.4244	.6531		.4687	.7054
	SparseLin		.4853	.7069		.5233	.7457
Deep LEARCH [29]	DNN		.4241	.6532		.4777	.7141
	DNN+SparseLin		.4682	.6781		.5220	.7300
BIRL [9, 32]	Linear	3.933	.4524	.6945	3.629	.4933	.7314
	SparseLin	26.840	.4900	.7084	8.975	.5375	.7508
Deep BIRL	DNN	3.621	.4617	.6958	3.308	.4973	.7340
	DNN+SparseLin	2.970	.4988	.7063	2.689	.5546	.7587
MaxEnt [53], MaxEnt++	Linear	4.4409	.4521	.6941	3.957	.4914	.7293
	SparseLin	26.749	.4922	.7092	8.876	.5401	.7522
Deep MaxEnt [46]	DNN	3.729	.4544	.6864	3.493	.4961	.7308
	DNN+SparseLin	2.889	.5007	.7062	2.920	.5490	.7516
RHIP	Linear	3.930	.4552	.6965	3.630	.4943	.7319
	SparseLin	26.748	.4926	.7095	8.865	.5408	.7522
	DNN	3.590	.4626	.6955	3.295	.5000	.7343
	DNN+SparseLin	2.881	**.5030**	.7086	2.661	**.5564**	.7591
Global ETA	Linear		.3891	.6538			
Global ETA+penalties	Linear		.4283	.6907			
Global RHIP	DNN+SparseLin	8.194	**.4958**	**.7208**			

steps. The stochastic policy π_s is both expensive to estimate (backward pass) and roll-out (forward pass) compared to the deterministic policy π_d, which can be efficiently computed via Dijkstra's algorithm.

Graph compression We introduce two graph compression techniques to reduce both the memory footprint and FLOP count across all IRL algorithms. The graph adjacency matrix is represented by a $B \times S \times V$ tensor, where entry (b,s,v) contains the reward of the v'th edge emanating from node s in batch sample b. Thus, V is the maximum node degree valency, and nodes with fewer than V outgoing edges are padded. For many problems, V is tightly bounded, e.g. typically $V < 10$ in road networks. First, we perform lossless compression by 'spliting' nodes with degree close to V into multiple nodes with lower degree. Since the majority of nodes have a much smaller degree than V, this slightly increases S but can significantly decrease the effective V, thus reducing the overall tensor size BSV in a lossless fashion. Second, we perform lossy compression by 'merging' nodes with a single outgoing edge into its downstream node as there is only one feasible action. Feature vectors of the merged nodes are summed, which is lossless for linear r_θ but introduces approximation error in the nonlinear setting. Intuitively, these compression techniques balance the graph's node degree distribution to reduce both the tensor padding (memory) and FLOP counts.

5 Empirical Study

Road graph Our 200M state MDP is created from the Google Maps road network graph. Edge features contain predicted travel duration (estimated from historical traffic) and other relevant static road properties, including distance, surface condition, speed limit, name changes and road type.

Demonstration dataset Dataset $\mathcal{D}$ contains de-identified users' trips collected during active navigation mode [20]. We filter for data quality by removing trips which contain loops, have poor GPS quality, or are unusually long. The dataset is a fixed-size subsample of these routes, spanning a period of two weeks and evenly split into training and evaluation sets based on date. Separate datasets are created for driving and two-wheelers, with the two-wheeler (e.g. mopeds, scooters) dataset being significantly smaller than the drive dataset due to a smaller region where this feature is available. The

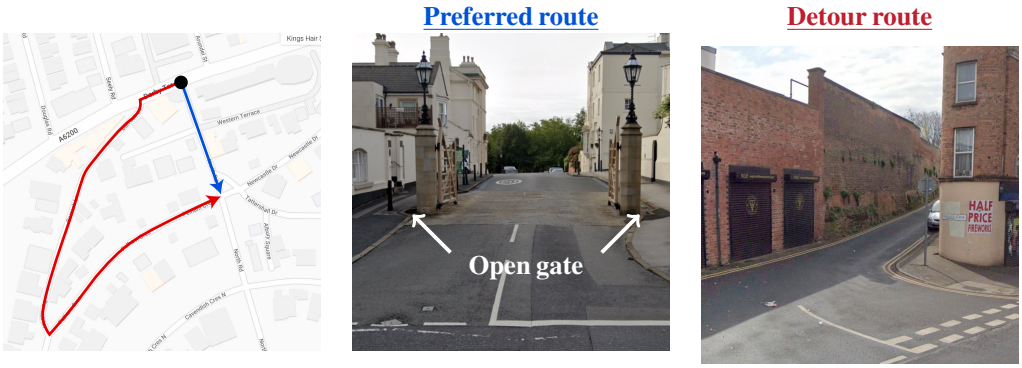

Figure 4: Example of the 360M parameter sparse model finding and correcting a data quality error in Nottingham. The preferred route is incorrectly marked as private property due to the presence of a gate (which is never closed), and incorrectly incurs a high cost. The detour route is long and narrow. The sparse model learns to correct the data error with a large positive reward on the gated segment. Additional examples are provided in Appendix D.

total number of iterated training and validation demonstration routes are 110M and 10M, respectively. See Appendix D for details.

Experimental region Due to the high computational cost of training the global model, we perform initial hyperparameter selection on a smaller set of 9 experimental metros (Bekasi, Cairo, Cologne, Kolkata, Manchester, Manila, Nottingham, Orlando, and Syracuse). The top-performing configuration is used to train the global driving model. Two-wheeler data is unavailable globally and thus not reported.

Baselines We evaluate both manually designed and IRL baselines. For fixed baselines, we consider (1) `ETA`: The fastest route, i.e. edge costs are the predicted travel duration and (2) `ETA+penalties`: ETA plus manually-tuned penalties for intuitively undesirable qualities (e.g. u-turns, unpaved roads), delivered to us in a closed form without visibility into the full set of underlying features. For IRL policy baselines, we compare MaxEnt (Algorithm 2) [54], Deep MaxEnt [47], the LEARCH [35] variation of MMP [34] (Algorithm 4), Deep LEARCH [29], and the maximum a posteriori variation of BIRL [9] (Algorithm 3). We also consider a deep version of BIRL similar to Brown and Niekum [6].

Reward model descriptions We evaluate three MoE function approximator classes: (1) a simple linear model, (2) a dense neural network (DNN) and (3) an ℓ_1-regularized reward parameter for every edge in the graph (SparseLin). The latter is of particular interest because it tends to highlight data-quality issues, for example in Figure 4. These models have 3.9k, 144k, and 360M global parameters, respectively. We constrain model weights to produce non-positive rewards and fine-tune all models from the `ETA+penalties` baseline. DNN+SparseLin indicates additive DNN and SparseLin components. See Appendix D.2 for details.

Metrics For serving online routing requests, we are interested in the highest reward path from s_o to s_d path under r_θ (and not a probabilistic sample from π or a margin-augmented highest reward path). For accuracy, a route is considered correct if it perfectly matches the demonstration route. Intersection over Union (IoU) captures the amount of overlap with the demonstration route, and is computed based on unique edge ids. Negative log-likelihood (NLL) loss is reported where applicable.

5.1 Results

We train the final global policy for 1.4 GPU-years on a large cluster of V100 machines, which results in a significant 15.9% and 24.1% increase in route accuracy relative to the `ETA+penalties` baseline models for driving and two-wheelers, respectively. As shown in Table 1, this RHIP policy with the largest 360M parameter reward model achieves state-of-the-art results with statistically significant accuracy gains of 0.4% and 0.2% compared to the next-best driving and two-wheeler IRL policies, respectively.

We observe dynamic programming convergence issues and large loss spikes in MaxEnt which tend to occur when the rewards become close to zero. In Appendix B we prove this phenomena occurs precisely when the dominant eigenvalue of the graph drops below a critical threshold of 1 (briefly noted in Ziebart [53, pg. 117]) and show the set of allowable θ is provably convex in the linear case. Fortunately, we

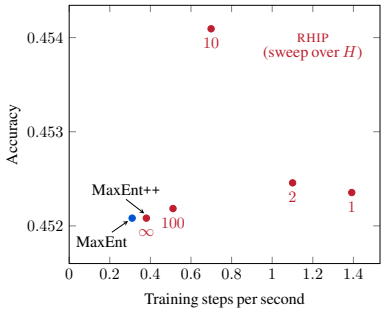

Figure 5: Impact of the horizon on accuracy and training time. $H = 10$ has the highest accuracy and trains 70% faster than MaxEnt.

Graph compression	N	V	Steps per sec	NLL	Acc
None	124,402	4.9	.373	9.371	.454
Split	125,278	3.0	.412	9.376	.455
Merge	84,069	4.9	.843	9.381	.455
Split+Merge	84,944	3.0	**.993**	9.389	.455

Table 2: Graph compression improves training time by 2.7x with insignificant impact on route quality metrics.

are able to manage the issue with careful initialization, learning rates, and stopping conditions. Note that RHIP (for $H < \infty$), BIRL and MMP provably do not suffer from this issue. All value functions (Algorithms 1, 2 and 3) are computed in log-space to avoid significant numerical stability issues.

We empirically study the trade-off between the use of cheap, deterministic planners and more robust yet expensive stochastic policies in Figure 5. As expected, MaxEnt has high accuracy but is slow to train due to expensive dynamic programming, and MaxEnt++ is 16% faster with no drop in accuracy. RHIP enables realizing a broad set of policies via the choice of H. Interestingly, we find that $H{=}10$ provides both the best quality routes and 70% faster training times than MaxEnt, i.e. MaxEnt is not on the Pareto front. We hypothesize this occurs due to improved policy specification. BIRL and MaxEnt assume humans probabilistically select actions according to the highest reward path or reward of all paths beginning with the respective state-action pair, respectively. However, in practice, humans may take a mixed approach – considering all paths within some horizon, and making approximations beyond that horizon.

Table 2 shows the impact of graph compression in our experimental region. The `split` strategy is lossless (as expected), and the `split+merge` strategy provides a significant 2.7x speed-up with almost no impact on route quality metrics. All empirical results take advantage of the `split+merge` graph compression. We find that data structure choice has a significant impact on training time. We try using unpadded, coordinate format (COO) sparse tensors to represent the graph adjacency matrix, but profiling results in our initial test metro of Bekasi show it to be 50x slower.

In Figure 6, we study the local geographic preferences learned by each expert in the mixture by performing an out-of-region generalization test. The drop in off-diagonal performance indicates the relative significance of local preferences. In Figure 7, we examine the relationship between region size and the performance of the model. Accuracy is nearly constant with respect to the number of states. However, training is significantly faster with fewer states, implying more equally sized regions would improve computational load balancing.

Negative results We study several other ideas which, unlike the above contributions, do not meaningfully improve scalability. First, the MaxEnt backward pass is equivalent to applying power iteration to solve for the dominant eigenvector of the graph (Equation 4). Instead of using power iteration (Algorithm 2), we consider using Arnoldi iteration from `ARPACK` [27], but find it to be numerically unstable due to lacking a log-space implementation (see results in Appendix A.1). Second, the forward pass used in MaxEnt has a closed form solution via the matrix geometric series (Equation 6). Using `UMFPACK` [11] to solve for this solution directly is faster on smaller graphs containing up to around 10k nodes, but provides no benefit on larger graphs (see results in Appendix A.2).

6 Discussion

Future research We study multiple techniques for improving the scalability of IRL and believe there exist several future directions which could lead to additional gains. First, demonstration paths with the same (or nearly the same) destination can be merged together into a single sample. Instead of performing one IRL backward and forward pass per mini-batch sample, we can now perform one iteration *per destination*. This enables compressing large datasets and increasing the effective batch size, although it reduces shuffling quality, i.e. samples are correlated during training. Second, the graph could be pruned by removing nodes not along a 'reasonable' path (i.e. within some margin of

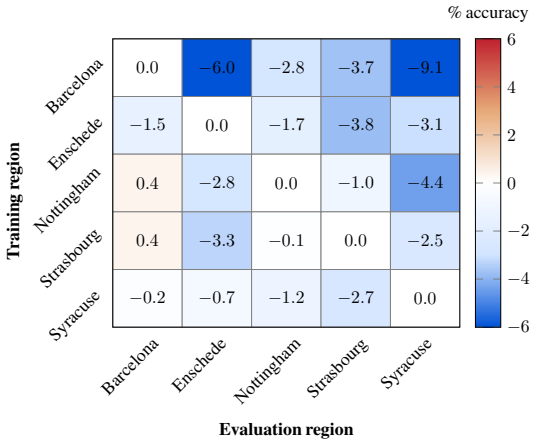

Figure 6: Sparse mixture-of-experts learn preferences specific to their geographic region, as demonstrated by the drop in off-diagonal performance.

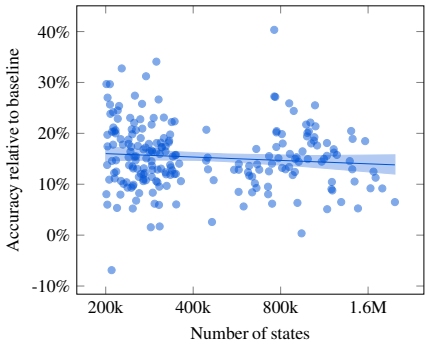

Figure 7: Region accuracy for each expert in the worldwide mixture. Performance is consistent across the state space size.

the current best path) from s_o to s_d [53, pg. 119]. However, this may be difficult to do in practice since the pruning is unique for every origin-destination pair.

From an accuracy perspective, we find that the sparse mixture-of-experts learn routing preferences specific to geographic regions. This vein could be further pursued with personalization, potentially via a hierarchical model [8, 10]. Due to engineering constraints, we use static ETA predictions, but would like to incorporate the dynamic GraphNet ETA predictions from Derrow-Pinion et al. [12]. We find that sparse reward models tend to highlight groups of edges which were impacted by the same underlying data quality issue. A group lasso penalty may be able to leverage this insight. Including human domain knowledge may robustify and help shape the reward function [48, 50]. In this paper, we evaluate performance on driving and two-wheelers, and would like to incorporate other modes of transportation – especially walking and cycling – but are limited by engineering constraints.

Extensions to other MDPs For expository purposes, we restrict attention to discrete, deterministic, and undiscounted MDPs with a single self-absorbing destination state. Our contributions naturally extend to other settings. MaxEnt++ and RHIP can be applied to any MDP where MaxEnt is appropriate and $v^{(0)}$ can be (efficiently) computed, e.g. via Dijkstra's. Our parallelization extends to all MDPs with a reasonable partition strategy, and the graph compression extends to stochastic MDPs (and with further approximation, discounted MDPs).

Limitations IRL is limited by the quality of the demonstration routes. Even with significant effort to remove noisy and sub-optimal routes from $\mathcal{D}$, our policy will inadvertently learn some rewards which do not reflect users' true latent preferences. Our MoE strategy is based on *geographic regions*, which limits the sharing of information across large areas. This could be addressed with the addition of global model parameters. However, global parameters would create undesirable dependencies during training, and the abundance of demonstrations and lack of correlation between region size and accuracy (Figure 7) suggests benefits may be minimal.

7 Conclusion

Increasing performance via increased scale – both in terms of dataset size and model complexity – has proven to be a persistent trend in machine learning. Similar gains for inverse reinforcement learning problems have historically remained elusive, largely due to additional challenges posed by scaling the MDP solver. We contribute both (a) techniques for scaling IRL to problems with hundreds of millions of states, demonstration trajectories, and reward parameters and (b) a novel generalization that provides a new view on classic IRL methods and enables fine-grained control over accuracy and planning time trade-offs. Our final policy is applied in a large scale setting with hundreds of millions of states and demonstration trajectories, which to the best of our knowledge represents the largest published benchmark of IRL algorithms in a real-world setting to date.

Acknowledgments

We gratefully acknowledge the contributions of Renaud Hartert, Rui Song, Thomas Sharp, Rémi Robert, Zoltan Szego, Beth Luan, Brit Larabee and Agnieszka Madurska towards an early exploration of this project for cyclists. Arno Eigenwillig provided useful suggestions for the graph's padded data structure, Jacob Moorman provided insightful discussions on the theoretical aspects of eigenvalue solvers, Jonathan Spencer provided helpful references for MaxEnt's theoretical analysis, and Ryan Epp explored the feasibility of an alternative approach to re-rank a small set of candidate routes. We are thankful for Remi Munos', Michael Bloesch's and Arun Ahuja's feedback on final iterations of this work.

References

[1] Pieter Abbeel et al. "Apprenticeship Learning for Motion Planning with Application to Parking Lot Navigation". In: *International Conference on Intelligent Robots and Systems* (2008).

[2] David Arthur and Sergei Vassilvitskii. *k-means++: The Advantages of Careful Seeding*. 2006.

[3] Chris L Baker, Rebecca Saxe, and Joshua B Tenenbaum. "Action Understanding as Inverse Planning". In: *Cognition* (2009).

[4] Andrew G Barto, Steven J Bradtke, and Satinder P Singh. "Learning to Act using Real-Time Dynamic Programming". In: *Artificial Intelligence* (1995).

[5] Stephen Boyd and Lieven Vandenberghe. *Convex Optimization*. Cambridge University Press, 2004.

[6] Daniel S. Brown and Scott Niekum. "Deep Bayesian Reward Learning from Preferences". In: *ArXiv* (2019).

[7] Alex J. Chan and Mihaela van der Schaar. "Scalable Bayesian Inverse Reinforcement Learning". In: *International Conference on Learning Representations* (2021).

[8] Jaedeug Choi and Kee-Eung Kim. "Hierarchical Bayesian Inverse Reinforcement Learning". In: *IEEE Transactions on Cybernetics* (2014).

[9] Jaedeug Choi and Kee-Eung Kim. "MAP Inference for Bayesian Inverse Reinforcement Learning." In: *Neural Information Processing Signals* (2011).

[10] Jaedeug Choi and Kee-Eung Kim. "Nonparametric Bayesian Inverse Reinforcement Learning for Multiple Reward Functions". In: *Neural Information Processing Systems* (2012).

[11] Timothy A Davis. "Algorithm 832: UMFPACK V4.3 - an Unsymmetric-pattern Multifrontal Method". In: *ACM Transactions on Mathematical Software (TOMS)* (2004).

[12] Austin Derrow-Pinion et al. "ETA Prediction with Graph Neural Networks in Google Maps". In: *International Conference on Information & Knowledge Management* (2021).

[13] *Difference of Proportion Hypothesis Test*. 2009. URL: `https://itl.nist.gov/div898/software/dataplot/refman2/auxillar/diffprop.htm`.

[14] Chelsea Finn, Sergey Levine, and Pieter Abbeel. "Guided Cost Learning: Deep Inverse Optimal Control via Policy Optimization". In: *International conference on machine learning* (2016).

[15] Chelsea Finn et al. "A Connection Between Generative Adversarial Networks, Inverse Reinforcement Learning, and Energy-Based Models". In: *arXiv:1611.03852* (2016).

[16] Divyansh Garg et al. "IQ-Learn: Inverse Soft-Q Learning for Imitation". In: *Neural Information Processing Systems* (2021).

[17] Robert Geisberger et al. "Exact Routing in Large Road Networks using Contraction Hierarchies". In: *Transportation Science* (2012).

[18] Jonathan Ho and Stefano Ermon. "Generative Adversarial Imitation Learning". In: *Neural Information Processing Systems* (2016).

[19] Roger A. Horn and Charles R. Johnson. *Matrix Analysis*. Cambridge University Press, 2012.

[20] *How Navigation Data Makes Maps Better for Everyone*. URL: `https://support.google.com/maps/answer/10565726`.

[21] John H. Hubbard and Barbara Burke Hubbard. "Vector Calculus, Linear Algebra, and Differential Forms: A Unified Approach". In: *The American Mathematical Monthly* (2003).

[22] Mahdi Imani and Ulisses M. Braga-Neto. "Control of Gene Regulatory Networks using Bayesian Inverse Reinforcement Learning". In: *Transactions on Computational Biology and Bioinformatics* (2019).

[23] R. E. Kalman. "When is a Linear Control System Optimal?" In: *Journal of Fluids Engineering, Transactions of the ASME* (1964).

[24] Liyiming Ke et al. "Imitation Learning as f-divergence Minimization". In: *Algorithmic Foundations of Robotics* (2021).

[25] J.F.C. Kingman. "A Convexity Property of Positive Matrices". In: *The Quarterly Journal of Mathematics* (1961).

[26] Kris M. Kitani et al. "Activity Forecasting". In: *European Conference on Computer Vision* (2012).

[27] Richard B Lehoucq, Danny C Sorensen, and Chao Yang. *ARPACK Users' Guide: Solution of Large-scale Eigenvalue Problems with Implicitly Restarted Arnoldi Methods*. 1998.

[28] James MacGlashan and Michael L Littman. "Between Imitation and Intention Learning". In: *International Joint Conference on Artificial Intelligence* (2015).

[29] Jim Mainprice et al. "Functional Nanifold Projections in Deep-LEARCH". In: *NeurIPS Workshop Neurorobotics*. 2016.

[30] Bernard Michini, Mark Cutler, and Jonathan P How. "Scalable Reward Learning from Demonstration". In: *International Conference on Robotics and Automation* (2013).

[31] Takayuki Osa et al. "An Algorithmic Perspective on Imitation Learning". In: *Foundations and Trends in Robotics* (2018).

[32] Deepak Ramachandran and Eyal Amir. "Bayesian Inverse Reinforcement Learning." In: *International Joint Conferences on Artificial Intelligence* (2007).

[33] Nathan D. Ratliff, J. Andrew Bagnell, and Siddhartha S. Srinivasa. "Imitation Learning for Locomotion and Manipulation". In: *International Conference on Humanoid Robots* (2007).

[34] Nathan D. Ratliff, J. Andrew Bagnell, and Martin A. Zinkevich. "Maximum Margin Planning". In: *International Conference on Machine Learning* (2006).

[35] Nathan D. Ratliff, David Silver, and J. Andrew Bagnell. "Learning to Search: Functional Gradient Techniques for Imitation Learning". In: *Autonomous Robots* (2009).

[36] Nicholas Rhinehart and Kris M. Kitani. "First-Person Activity Forecasting from Video with Online Inverse Reinforcement Learning". In: *Transactions on Pattern Analysis and Machine Intelligence* (2020).

[37] Stéphane Ross and Drew Bagnell. "Efficient Reductions for Imitation Learning". In: *International Conference on Artificial Intelligence and Statistics* (2010).

[38] Stéphane Ross, Geoffrey Gordon, and Drew Bagnell. "A reduction of imitation learning and structured prediction to no-regret online learning". In: *International Conference on Artificial Intelligence and Statistics* (2011).

[39] John Rust. "Structural Estimation of Markov Decision Processes". In: *Handbook of Econometrics* (1994).

[40] Noam Shazeer et al. "Outrageously Large Neural Networks: The Sparsely-Gated Mixture-of-Experts Layer". In: *International Conference on Learning Representations* (2017).

[41] Gokul Swamy et al. "Inverse Reinforcement Learning without Reinforcement Learning". In: *International Conference on Machine Learning* (2023).

[42] Gokul Swamy et al. "Of Moments and Matching: A Game-Theoretic Framework for Closing the Imitation Gap". In: *International Conference on Machine Learning* (2021).

[43] Bulent Tastan and Gita Sukthankar. "Learning Policies for First Person Shooter Games using Inverse Reinforcement Learning". In: *Conference on Artificial Intelligence and Interactive Digital Entertainment* (2011).

[44] Lloyd N. Trefethen and David Bau. *Numerical Linear Algebra*. SIAM, 1997.

[45] Aaron Tucker, Adam Gleave, and Stuart Russell. "Inverse Reinforcement Learning for Video Games". In: *arXiv:1810.10593* (2018).

[46] Larry Wasserman. *All of Statistics: A Concise Course in Statistical Inference*. Springer, 2004.

[47] Markus Wulfmeier, Peter Ondruska, and Ingmar Posner. "Maximum Entropy Deep Inverse Reinforcement Learning". In: *arXiv:1507.04888* (2015).

[48] Markus Wulfmeier, Dushyant Rao, and Ingmar Posner. "Incorporating Human Domain Knowledge into Large Scale Cost Function Learning". In: *ArXiv* (2016).

[49] Markus Wulfmeier, Dominic Zeng Wang, and Ingmar Posner. "Watch This: Scalable Cost-function Learning for Path Planning in Urban Environments". In: *International Conference on Intelligent Robots and Systems* (2016).

[50] Markus Wulfmeier et al. "Large-scale Cost Function Learning for Path Planning using Deep inverse reinforcement Learning". In: *The International Journal of Robotics Research* (2017).

[51] Yue Xing, Qifan Song, and Guang Cheng. "On the Algorithmic Stability of Adversarial Training". In: *Neural Information Processing Systems* (2021).

[52] Chao Yu, Guoqi Ren, and Jiming Liu. "Deep Inverse Reinforcement Learning for Sepsis Treatment". In: *International Conference on Healthcare Informatics* (2019).

[53] Brian D. Ziebart. "Modeling Purposeful Adaptive Behavior with the Principle of Maximum Causal Entropy". 2010.

[54] Brian D. Ziebart et al. "Maximum Entropy Inverse Reinforcement Learning". In: *AAAI Conference on Artificial Intelligence* (2008).

Appendix for "Massively Scalable Inverse Reinforcement Learning in Google Maps"

Notation Let $R \in \mathbb{R}^{|\mathcal{S}| \times |\mathcal{S}|}$ be the sparse reward matrix defined by $R_{ij} = r_\theta(s_i, s_j)$.

A Negative results

In this section, we provide negative results for two ideas to improve MaxEnt's scalability. We used a synthetic Manhattan-style street grid (i.e. GridWorld) in order to conduct controlled sweeps over the number of nodes. Edge rewards were fixed at constant values.

A.1 Arnoldi iteration

The backward pass in MaxEnt is equivalent to performing power iteration to compute the dominant eigenvector of the graph

$$A_{ij} = e^{R_{ij}}. \tag{4}$$

We attempted to use Arnoldi iteration, as implemented in `ARPACK`, but found it to be numerically unstable due to lacking a log-space version [27]. In typical eigenvector applications, one is concerned with the reconstruction error $||Az - z||$, where $z = e^v$ is an eigenvector estimate of A. However, in MaxEnt we are uniquely concerned with relative error between entries in rows of $Q = R + \mathbb{1} \cdot v^\intercal$, since this determines the policy $\pi = \mathrm{softmax}(Q)$. We found log-space reconstruction error $||\log(Az) - \log(z)||$ to be far more significant in MaxEnt. As seen in Figure 8, Arnoldi iteration's reconstruction error in linear space is reasonable, but quickly blows up in log space, unlike log-space power iteration.

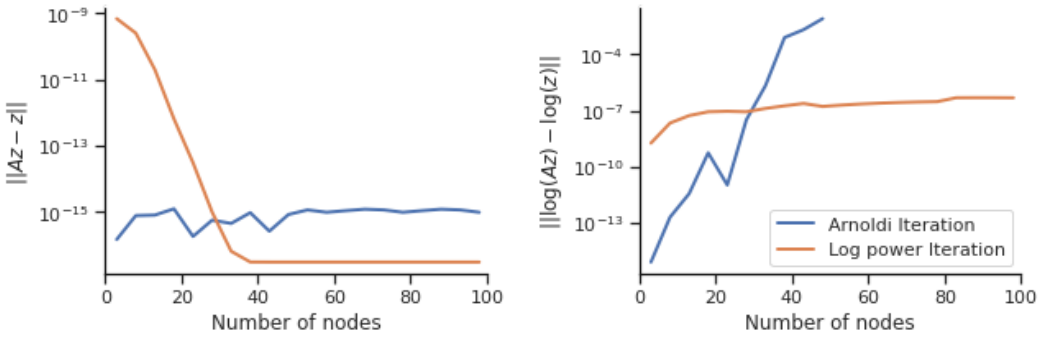

Figure 8: Solving for the dominant eigenvector in the MaxEnt backward pass.

From a geometric perspective, this phenomena can be observed by examining eigenvector estimates z in Figure 9. Due to the MDP structure containing a single absorbing zero-reward destination node, eigenvector entries z rapidly decay as one moves further away from the destination s_d. Thus, the typical reconstruction error $||Az - z||$ is primarily a function of a handful of nodes near the destination. Visually, Arnoldi and log-space power iteration appear to provide similar solutions for z. However, examining $\log(z)$ reveals that log-space power iteration is able to gracefully estimate the exponentially decaying eigenvector entries. Arnoldi iteration successfully estimates the handful of nodes near s_d, but further nodes are inaccurate and often invalid (white spaces indicate $z < 0$ and thus $\log(z)$ is undefined).

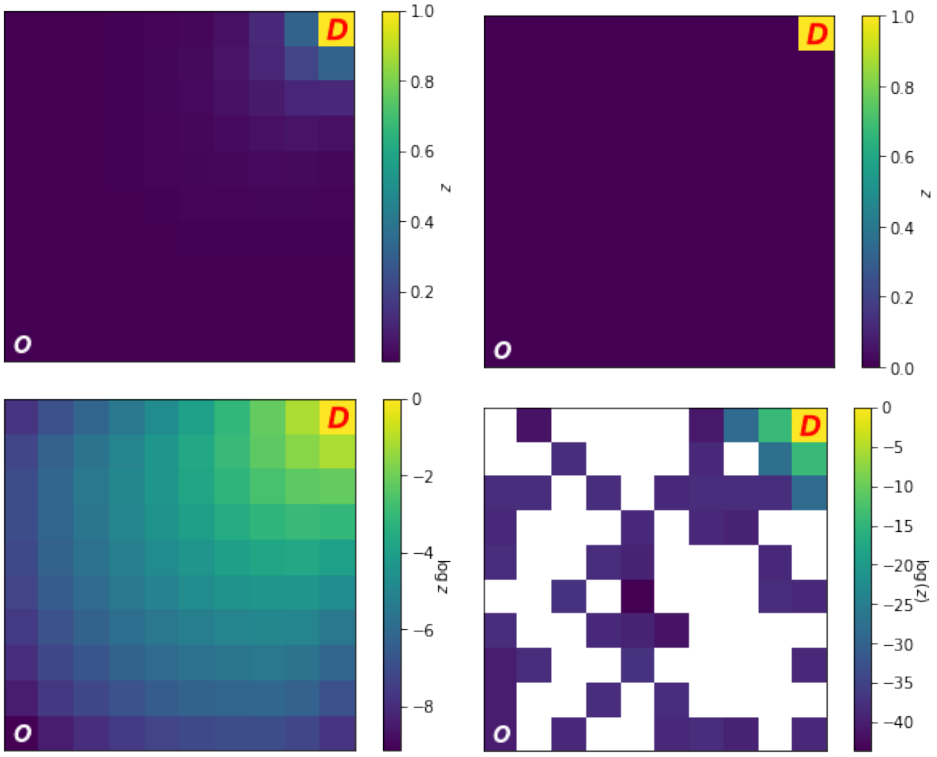

(a) Log power iteration (b) Arnoldi iteration

Figure 9: Eigenvector estimates on a 10×10 GridWorld environment for origin O and destination D.

A.2 Matrix geometric series

The MaxEnt forward pass is a matrix geometric series with the closed-form solution defined in Equation 6. Instead of iteratively computing the series, we used `UMFPACK` to directly solve for this solution. As shown in Figure 10, this worked very well for graphs up to approximately 10k nodes, but provided no further benefit beyond this point. Neither approach had numerical stability issues.

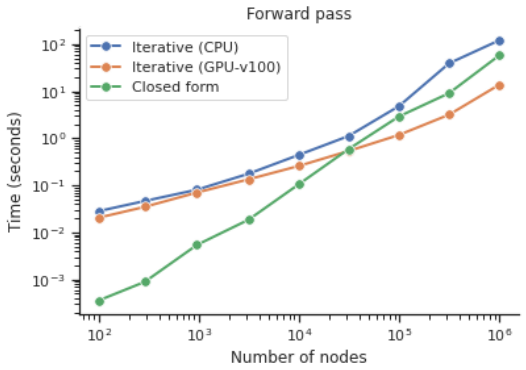

Figure 10: Closed-form solution of the MaxEnt forward pass using `UMFPACK`.

A.3 Negative designs

We dismiss two other designs based on key pieces of evidence. First, we could learn to rerank the $\sim$5 routes returned by the Maps API (the approach taken by Ziebart et al. [54]). This is a trivial solution to scale, but significantly reduces the route accuracy headroom. The API returns a handful of candidate routes from s_o to s_d, which then form $\mathcal{T}$, e.g. Equation 2 or Equation 3. Instead of learning the best route from a set of infinitely many routes, IRL now learns the best route among $\sim$5. In many cases, the desired

demonstration is often not among this set, and thus impossible to select in an online setting. Second, we could train in a smaller geographic region and deploy worldwide. Not only does this preclude the use of the best-performing 360M parameter sparse reward function (as its parameters are unique to each edge), Figure 6 indicates this would suffer from generalization error for other choices of r_θ.

B MaxEnt theory

In this section, we provide theoretical results on MaxEnt, which are summarized here for convenience:

- Theorem B.1: MaxEnt has finite loss if and only if the dominant eigenvalue $\lambda_{\max}$ of the graph is less than 1. This was briefly noted in Ziebart [53, pg. 117]), which we discovered after preparation of this publication.
- Theorem B.2: The set of finite losses is convex in the linear setting.
- Theorem B.3: The convergence rate of the backward pass is governed by the second largest eigenvalue.

Figure 11 illustrates the first two phenomena on a simple didactic MDP. Intuitively, there are two counteracting properties which determine the transition between finite and infinite loss. First, the number of paths of length $n+1$ is larger than the number of paths of length n. This tends to accumulate probability mass on the set of longer paths. Second, paths of length $n+1$ have on average lower per-path reward, and thus lower per-path probability, than paths of length n. This favors the set of shorter paths. The question is, does the per-path probability decrease faster than the rate at which the number of paths increases? If yes, then the dominant eigenvalue is 1, the forward pass converges, and the loss is finite. If no, then the dominant eigenvalue is greater than 1, the forward pass never converges, and loss is infinite. As expected, infinite loss occurs in regions of high edge rewards, which agrees with Figure 11.

B.1 Preliminaries

Let $A_{ij} = e^{R_{ij}}$ be the elementwise exponential rewards. We restrict our attention to linear reward functions $R_{ij} = \theta^\intercal x_{ij}$ where x_{ij} is set of edge features between nodes i and j. If no edge exists between nodes i and j, then the reward is negative infinite and $A_{ij} = 0$. Without loss of generality, we assume the destination node is the last row in A. Thus, A is block upper triangular (also called the *irreducible normal form* or *Frobenius normal form*)

$$A = \begin{bmatrix} B_1 & * \\ 0 & B_2 \end{bmatrix}$$

where B_1 contains all the non-destination nodes and $B_2 = [1]$ is the self-absorbing destination node. B_1 and B_2 are both strongly connected (thus irreducible) and regular. B_2 has a single eigenvalue $\lambda_{\max}(B_2) = 1$, and by the Perron-Frobenius theorem B_1 has a dominant real eigenvalue $\lambda_{\max}(B_1)$ (called the Perron-Frobenius eigenvalue of B_1).

Likewise, we express an eigenvector z of A as

$$\begin{bmatrix} B_1 & * \\ 0 & B_2 \end{bmatrix} \begin{bmatrix} z_1 \\ z_2 \end{bmatrix} = \lambda \begin{bmatrix} z_1 \\ z_2 \end{bmatrix} \tag{5}$$

and the MaxEnt policy transition matrix as

$$\pi = \begin{bmatrix} P_1 & * \\ 0 & P_2 \end{bmatrix}$$

where $P_2 = [1]$ corresponds to the self-absorbing edge at the destination, and P_1 corresponds to all other nodes.

The MaxEnt backward pass is unnormalized power iteration. After k iterations, $z^{(k)} = A^k \mathbb{I}_{s_d}$ where $\mathbb{I}_{s_d}$ is the one-hot vector at the destination node. This is exactly (unnormalized) power iteration.

Likewise, the forward pass is a matrix geometric series. The *fundamental matrix* S [21] is defined as

$$\begin{aligned} S &= I + P_1 + P_1^2 + \cdots \\ &= (I - P_1)^{-1} \end{aligned} \tag{6}$$

Then the forward pass is simply $\mathbb{I}_{s_o}^\intercal S$, where $\mathbb{I}_{s_o}$ is the one-hot vector at the origin. If P_1 is sub-stochastic, then the series converges and $(I - P_1)$ is nonsingular. With these preliminaries, we now proceed to our main results.

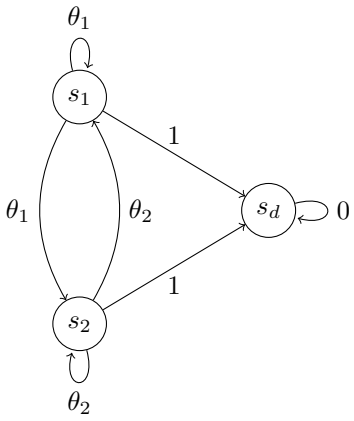

(a) Simple MDP

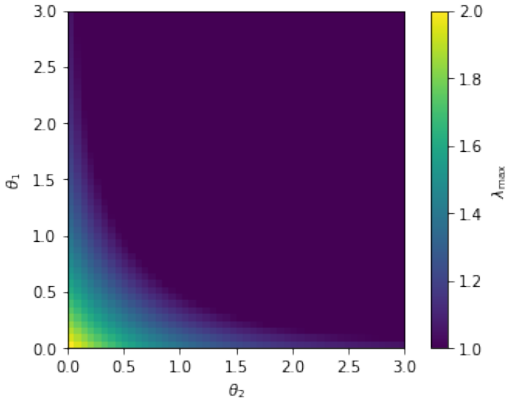

(b) Dominant eigenvalue

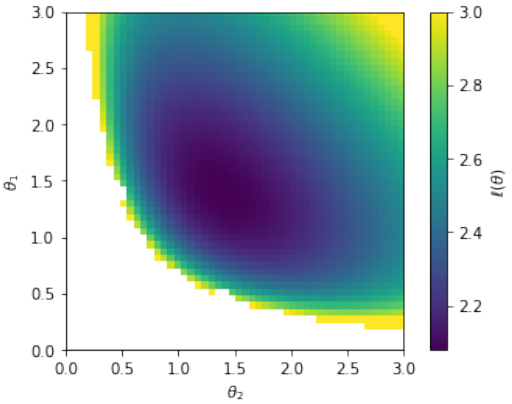

(c) MaxEnt loss

Figure 11: Demonstration of our claims on a simple MDP. (a) The deterministic MDP with absorbing destination node s_d, and parameterized edge costs (i.e. negative reward) θ_1 and θ_2. (b) The dominant eigenvalue of the graph as a function of θ. Note the set of parameters $\Theta = \{\theta : \lambda_{\max}(\theta) = 1\}$ is convex. (c) The corresponding MaxEnt loss (for a dataset with two demonstration paths $s_1 \to s_2 \to s_d$ and $s_2 \to s_1 \to s_d$). As explained by our theory, the loss is finite and convex when $\lambda_{\max} = 1$ and infinite when $\lambda_{\max} > 1$.

B.2 Main results

Theorem B.1. *$\ell(\theta) < \infty$ iff A has a dominant eigenvalue of 1.*

Proof. The spectrum of A, denoted $\sigma(A)$, is the union of $\sigma(B_1)$ and $\sigma(B_2)$, including multiplicities.[7] Thus, there are three possible cases:

1. **Case 1**: $\lambda_{\max}(B_1) < 1$. In this case, there exists a dominant eigenvector with eigenvalue 1 from B_2. This eigenvector must satisfy $z_2 > 0$ (proof by contradiction: assume $z_2 = 0$, then $B_1 z_1 = z_1$, which contradicts $\lambda_{\max}(B_1) < 1$). Since $z_2 > 0$, P_1 is substochastic (there is some probability of transitioning to the destination node), the matrix geometric series $(I + P_1 + P_1^2 + \cdots)$ converges, and the loss is finite.
2. **Case 2**: $\lambda_{\max}(B_1) > 1$. There exists a dominant eigenvector with eigenvalue $\lambda_{\max}(B_1)$. Then by Equation 5, z_2 must equal zero. By the MaxEnt policy definition, the policy will never transition to the destination ($\pi_{iN} = 0 \; \forall i \neq N$), the forward pass geometric series diverges, and thus $\ell(\theta) = \infty$.

[7] by 8.3.P8 in Horn and Johnson [19]

3. **Case 3**: $\lambda_{\max}(B_1) = 1$. This determines whether the set is open or closed. We do not address this question in this paper, although we strongly suspect the set is open.

In both Cases 1 and 2, there exists a dominant eigenvector. By standard power iteration analysis, the MaxEnt backward pass is guaranteed to converge to this dominant eigenvector. The MaxEnt loss $\ell(\theta)$ is finite in Case 1 when A has a dominant eigenvalue of 1, and infinite in Case 2. □

Computing the dominant eigenvalue may be expensive. Fortunately, it is often possible to cheaply verify Case 1 holds by use of the following simple inequalities[8]

$$\lambda_{\max}(B_1) \leq \max_i r_i \sum_j B_{1,ij} r_j \leq \max_i r_i$$

$$\lambda_{\max}(B_1) \leq \max_j c_j \sum_i B_{1,ij} c_i \leq \max_j c_j$$

where $r_i = \sum_j B_{1,ij}$ and $c_j = \sum_i B_{1,ij}$ are the row and column sums, respectively.

Theorem B.2. $\Theta = \{\theta : \ell(\theta) < \infty\}$ *is an open convex set.*

Proof. From the proof of Theorem B.1, we have the equivalence

$$\Theta = \{\theta : \lambda_{\max}(B_1) < 1\}. \tag{7}$$

Let

$$\lambda_{\max}(B_1) = h(g(f(\theta)))$$

where

Definition	Name	Relevant properties
$f(\theta) = X\theta$	Edge rewards	Linear
$g(R) = e^R$	Elementwise exponential	Convex, increasing
$h(B_1) = \lambda_{\max}(B_1)$	Dominant eigenvalue	Log-convex, increasing

The only non-obvious fact is that h is convex and increasing. Log-convexity follows from Kingman [25]. It is increasing by the Perron-Frobenius theorem for non-negative irreducible matrices.

The proof follows standard convexity analysis [5]. The function $g \circ f$ is convex since f is convex and g is convex and increasing. The function $h \circ g \circ f$ is convex since $g \circ f$ is convex and h is convex and increasing. Finally, since $\lambda_{\max}(B_1) = h \circ g \circ f$ is convex in θ, the sublevel set in Equation 7 is also convex. □

Theorem B.3. *The error of the MaxEnt backward pass after k iterations is*

$$||z^{(k)} - z|| = \mathcal{O}\left(\left|\frac{\lambda_2}{\lambda_1}\right|^k\right) \tag{8}$$

where λ_1 is the dominant eigenvalue of A ($\lambda_1 = 1$ in Case 1), and $\lambda_2 < \lambda_1$ is the second largest eigenvalue.

Proof. This follows directly from standard power iteration analysis, e.g. Theorem 27.1 in Trefethen and Bau [44]. □

B.3 Proof of Equation 2

In Section 4, we claim our MaxEnt++ initialization is closer to the desired solution than the original MaxEnt initialization

$$\underbrace{\mathbb{I}_{s=s_d}}_{\text{MaxEnt initialization}} \quad \leq \quad \underbrace{\min_{\tau \in \mathcal{T}_{s,s_d}} e^{r(\tau)}}_{\text{MaxEnt++ initialization}} \quad \leq \quad \underbrace{\sum_{\tau \in \mathcal{T}_{s,s_d}} e^{r(\tau)} = v}_{\text{Solution}}$$

The MaxEnt initialization $\mathbb{I}_{s=s_d}$ is zero everywhere, except at s_d where it equals one. The MaxEnt++ initialization $\min_{\tau \in \mathcal{T}_{s,s_d}} e^{r(\tau)}$ is non-negative (due to the exponent), and is equal to one

[8] by Lemma 8.1.21 and 8.1.P7 in Horn and Johnson [19].

at s_d (since there is a single, zero-reward, self-absorbing edge at the destination). Thus, the MaxEnt++ initialization upper bounds the MaxEnt initialization. The solution $\sum_{\tau \in \mathcal{T}_{s,s_d}} e^{r(\tau)} = v$ upper bounds the MaxEnt++ initialization by the inequality $\min_x f(x) \leq \sum_x f(x)$, where $f(x) \geq 0 \ \ \forall x$.

Note the claim in Equation 2 is stronger than claiming a smaller vector distance.

C Baseline algorithms

In this section, we summarize the baseline IRL algorithms and provide reductions from RHIP.

C.1 MaxEnt++ and MaxEnt

MaxEnt [54] assumes a softmax distribution over trajectories.

$$\pi(\tau) \propto e^{r(\tau)} \tag{9}$$

$$\pi(a|s) \propto \sum_{\tau \in \mathcal{T}_{s,a}} e^{r(\tau)} \tag{10}$$

where $\mathcal{T}_{s,a}$ is the set of all trajectories which begin with state-action pair (s,a). Computing the gradient of the log-likelihood of Equation 9 results in dynamic programming Algorithm 2.

Algorithm 2 MaxEnt++ and MaxEnt

Input: Reward r_θ, demonstration τ with origin s_o and destination s_d
Output: Parameter update $\nabla_\theta f$

```
# Policy estimation
```
$v^{(0)}(s) \leftarrow \text{DIJKSTRA}(r_\theta, s, s_d)$ ▷ Equation 2. The original MaxEnt uses $\log \mathbb{I}[s = s_d]$
for $h = 1,2,...$ **do**
  $Q^{(h)}(s,a) \leftarrow r_\theta(s,a) + v^{(h-1)}(s')$
  $v^{(h)}(s) \leftarrow \log \sum_a \exp Q^{(h)}(s,a)$
end for
$\pi(a|s) \leftarrow \frac{\exp Q^{(h)}(s,a)}{\sum_{a'} \exp Q^{(h)}(s,a')}$ ▷ Equation 9

```
# Roll-out policy
```
$\rho^\theta \leftarrow \text{Rollout}(\pi, s_o)$

$\nabla_\theta f \leftarrow \sum_{s,a} (\rho_\tau(s,a) - \rho^\theta(s,a)) \nabla_\theta r_\theta(s,a)$
Return: $\nabla_\theta f$

The reduction from RHIP to MaxEnt follows directly from Equation 3 with $H = \infty$. Recall π_s is the MaxEnt++ policy after H iterations, and let π_∞ denote the fully converged MaxEnt++ policy (equivalent to the fully converged MaxEnt policy)

$$\begin{aligned}
\pi(a|s) &\propto \sum_{\tau \in \mathcal{T}_{s,a}} \pi_d(\tau_{H+1}) \prod_{h=1}^{H} \pi_s(a_h|s_h) && \text{RHIP} \\
&= \sum_{\tau \in \mathcal{T}_{s,a}} \prod_{h=1}^{\infty} \pi_\infty(a_h|s_h) \\
&= \sum_{\tau \in \mathcal{T}_{s,a}} \pi_\infty(\tau) && \text{MaxEnt++ and MaxEnt}
\end{aligned}$$

The careful reader will notice a subtle distinction between Algorithm 1 (RHIP) and Algorithm 2 (MaxEnt). The former computes the gradient via Equation 10, whereas the latter computes the gradient via Equation 9. The resulting gradients are identical, however, the latter results in a simpler algorithm. Mechanically, Algorithm 1 with $H = \infty$ reduces to the simpler Algorithm 2 via a telescoping series.

C.2 Bayesian IRL

Bayesian IRL [32] assumes the policy follows the form

$$\pi(a|s) \propto e^{Q^*(s,a)} \tag{11}$$

where $Q^*(s,a)$ is the Q-function of the optimal policy. In our setting, π_d is the optimal policy, and thus $Q^*(s,a)$ is the reward of taking (s,a) and then following π_d, i.e. $Q^{(0)}$ in Algorithm 1. Computing the gradient of the log-likelihood of Equation 11 results in Algorithm 3

Algorithm 3 Bayesian IRL

Input: Reward r_θ, demonstration τ with origin s_o and destination s_d
Output: Parameter update $\nabla_\theta f$

`# Backup policy`
$v(s) \leftarrow \text{DIJKSTRA}(r_\theta, s, s_d)$
$Q(s,a) \leftarrow r_\theta(s,a) + v(s')$
$\pi(a|s) \leftarrow \frac{\exp Q(s,a)}{\sum_{a'} \exp Q(s,a')}$ ▷ Equation 11

`# Roll-out policy`
$\rho^\theta \leftarrow \text{Rollout}(\pi, \rho^s_\tau)$
$\rho^* \leftarrow \text{Rollout}(\pi_{2:\infty}, \rho^s_{\tau_{2:\infty}}) + \rho^{sa}_\tau$

$\nabla_\theta f \leftarrow \sum_{s,a} (\rho^*(s,a) - \rho^\theta(s,a)) \nabla_\theta r_\theta(s,a)$
Return: $\nabla_\theta f$

The reduction from RHIP to BIRL directly follows from Equation 3 with $H=1$.

$$\begin{aligned}
\pi(a|s) &\propto \sum_{\tau \in \mathcal{T}_{s,a}} \pi_d(\tau_{H+1}) \prod_{h=1}^{H} \pi_s(a_h|s_h) && \text{RHIP} \\
&= \sum_{\tau \in \mathcal{T}_{s,a}} \pi_d(\tau_{H+1}) \pi_1(a_h|s_h) \\
&= \sum_{\tau \in \mathcal{T}_{H,s,a}} \pi_1(a_h|s_h) \\
&= \sum_{\tau \in \mathcal{T}_{H,s,a}} \pi_1(a_h|s_h) \\
&= e^{Q^{(0)}(s,a)} = e^{Q^*(s,a)} && \text{BIRL}
\end{aligned}$$

where $\mathcal{T}_{H,s,a}$ is the set of all paths which begin with a state-action pair (s,a) and deterministically follow the highest reward path after horizon H.

C.3 Max Margin Planning

Max Margin Planning [34, 35] assumes a loss ℓ of the form

$$\begin{aligned}
\ell(\theta) &= \underbrace{\sum_{s,a} \rho^{sa}_\tau(s,a) r_\theta(s,a)}_{\text{Demonstration path reward}} \underbrace{- \max_{\tau' \in \mathcal{T}} \sum_{s,a} \rho^{sa}_{\tau'}(s,a)(r_\theta(s,a) + m_\tau(s,a))}_{\text{Margin-augmented highest reward path}} \\
&= \sum_{s,a} (\rho_\tau(s,a) - \rho_{\tau_{\text{sp}}}(s,a)) r_\theta(s,a)
\end{aligned} \tag{12}$$

where $\mathcal{T}$ is the set of all paths from s_o to s_d, m_τ is the margin term, and τ_{sp} is the margin-augmented highest reward path, i.e. $\tau_{\text{sp}} = \text{DIJKSTRA}(r_\theta + m_\tau, s_o, s_d)$. The resulting MMP algorithm is shown in Algorithm 4.

Algorithm 4 Max Margin Planning (MMP)

Input: Reward r_θ, demonstration τ with origin s_o and destination s_d
Output: Parameter update $\nabla_\theta f$

```
# Estimate and roll-out policy
```
$\rho_{\tau_{\text{sp}}} \leftarrow \text{DIJKSTRA}(r_\theta + m_\tau, s_o, s_d)$ ▷ Equation 12

$\nabla_\theta f \leftarrow \sum_{s,a} (\rho_\tau(s,a) - \rho_{\tau_{\text{sp}}}(s,a)) \nabla_\theta r_\theta(s,a)$
Return: $\nabla_\theta f$

The reduction from RHIP to MMP is possible by directly examining Algorithm 1 with $H = 0$ and absorbing the margin term into the reward function, i.e. $r'(\theta) = r(\theta) + m_\tau$. With $H{=}0$, $\pi = \pi_d$ in Algorithm 1. Beginning with the $\rho^* - \rho^\theta$ term in Algorithm 1

$$
\begin{aligned}
\rho^* - \rho^\theta &= \text{Rollout}(\pi_{2:\infty}, \rho^s_{\tau_{2:\infty}}) + \rho^{sa}_\tau - \text{Rollout}(\pi, \rho^s_\tau) && \text{RHIP} \\
&= \text{Rollout}(\pi_d, \rho^s_{\tau_{2:\infty}}) + \rho^{sa}_\tau - \text{Rollout}(\pi_d, \rho^s_\tau) && H{=}0 \\
&= \rho^{sa}_\tau - \text{Rollout}(\pi_d, s_o) && \text{Telescoping series} \\
&= \rho^{sa}_\tau - \rho^{sa}_{\tau_{\text{sp}}} && \text{MMP}
\end{aligned}
$$

D Experiments

D.1 Dataset

The demonstration dataset contains 110M and 10M training and validation samples, respectively. Descriptive statistics of these routes are provided below.

Travel model	Distance (km)	Duration (min)	Road segments per demonstration
Drive	9.7	13.3	99.5
Two-wheeler	3.0	8.3	47.4

Table 3: Dataset summary statistics

GPS samples are matched to the discrete road graph using a hidden Markov model. For data cleaning, we relied on several experts who had at least 5 years of experience in curating routing databases. This is similar to data cleaning processes followed in prior work, for example in Derrow-Pinion et al. [12].

D.2 Hyperparameters

The full hyperparameter sweep used in Table 1 (excluding global result in bottom row) is provided in Appendix D.2.

Category	Hyperparameter	Values	Applicable methods
Policy	Softmax temperature	10, 20, 30	MaxEnt, BIRL
	Horizon	2, 10, 100	RHIP
	Margin	0.1, 0.2, 0.3	MMP
	Fixed bias	Margin+0.001	MMP
Reward model	Hidden layer width	18	DNN
	Hidden layer depth	2	DNN
	Initialization	$(1 \pm .02) * \texttt{ETA+penalties}$	Linear, DNN
	Weight initialization	0	SparseLin
	L1 regularization	1e-7	SparseLin
Optimizer	SGD learning rate	0.05, 0.01	Linear, DNN
	Adam learning rate	1e-5, 1e-6	SparseLin
	Adam β_1	0.99	SparseLin
	Adam β_2	.999	SparseLin
	Adam ϵ	1e-7	SparseLin
	LR warmup steps	100	All
Training	Steps per epoch	100	All
	Batch size	8	All
	Epochs	200, 400	All
Data compression	Max out degree	3	All

Table 4: Hyperparameters.

The worldwide 360M parameter RHIP model (bottom row of Table 1) uses the same parameters as Appendix D.2, except that we only swept over the horizon parameter in $H \in \{10,100\}$ and the SGD learning rate, for efficiency. Temperature was fixed at 30 for linear and 10 for sparse. Adam learning rate was fixed at 0.05.

D.3 Statistical significance analysis

The p-values for Table 1 are computed as follows:

Accuracy We used a two-sided difference of proportions test [13]. Our validation set in the experimental region contains $n = 360,000$ samples. RHIP outperforms the next-best drive and two-wheeler policies by .0023 (p-value=.051) and .0018 (p-value=.122), respectively. Note that since policies share a validation set, the routes on which they have a perfect match are not independent but likely positively correlated, making these estimates conservative.

IoU We used a Hoeffding bound to construct a confidence interval for the difference of IoU scores [46]. We find RHIP does not provide a statistically significant improvement.

D.4 Additional results

(a) **Spokane** A road is incorrectly marked as drivable. The correct route takes users through the designated drive-through, as desired. The sparse model learns to correct the data error with a large negative reward on the flex-posts segment.

(b) **Syracuse** Similar to Figure 4, except this road segment is *occasionally* closed. The longer detour follows several back roads and parking lots.

Figure 12: Examples of the 360M parameter sparse model finding and correcting data quality errors. Locations were selected based on the largest sparse reward magnitudes in the respective regions.